

Article

Robust Medical Image Watermarking Scheme Using PSO, LWT, and Hessenberg Decomposition

Lalan Kumar ^{1,†}, Kamred Udham Singh ^{1,*}, Indrajeet Kumar ^{2,†} , Ankit Kumar ^{3,†} and Teekam Singh ^{4,†} ¹ School of Computing, Graphic Era Hill University, Dehradun 248002, India² Department of Computer Science and Engineering, Graphic Era Hill University, Dehradun 248002, India³ Department of Computer Engineering and Application, GLA University, Mathura 281406, India; iiita.ankit@gmail.com⁴ Department of Computer Science and Engineering, Graphic Era Deemed to Be University, Dehradun 248002, India* Correspondence: 11004033@gs.ncku.edu.tw

† These authors contributed equally to this work.

Abstract: Digital imaging is a technology that is extensively employed in diverse diagnostic examinations such as magnetic resonance imaging (MRI), computed tomography (CT), and ultrasound imaging, among other modalities. Transferring a patient's diagnostic images and medical data to a specialist physician in a distinct geographical location is conducted to facilitate an accurate diagnosis. The safeguarding of patient data privacy and confidentiality is ensured through the utilisation of smart hospital applications for medical data security. The current research presents the effective utilisation of lifting wavelet transform (LWT) and Hessenberg-based particle swarm optimization in order to generate resilient and safeguarded watermarks on ultrasound images. The empirical evidence suggests that our innovative approach outperforms our prior methodology, established through extensive testing. The watermark's imperceptibility and accuracy are exemplified by its capacity to sustain a superior structural similarity index measure (SSIM) and peak signal-to-noise ratio (PSNR), even amidst diverse image processing assaults.

Keywords: LWT; authentication; medical image; PSO; Hessenberg decomposition

Citation: Kumar, L.; Singh, K.U.; Kumar, I.; Kumar, A.; Singh, T. Robust Medical Image Watermarking Scheme Using PSO, LWT, and Hessenberg Decomposition. *Appl. Sci.* **2023**, *13*, 7673. <https://doi.org/10.3390/app13137673>

Academic Editor: Mostafa Fouda

Received: 27 May 2023

Revised: 20 June 2023

Accepted: 20 June 2023

Published: 28 June 2023



Copyright: © 2023 by the authors. Licensee MDPI, Basel, Switzerland. This article is an open access article distributed under the terms and conditions of the Creative Commons Attribution (CC BY) license (<https://creativecommons.org/licenses/by/4.0/>).

1. Introduction

The development of electronic healthcare systems in smart cities and the support of the medical community have gained popularity over the past decade. In electronic healthcare systems, medical information such as medical reports and images (i.e., USG, CT scan, MRI, or X-ray) is transmitted via interactive audiovisual medium for the purpose of consultation and occasionally for distant medical operations or tests. The medical images used in an electronic healthcare system are extremely vulnerable to any data breach since they contain sensitive patient information required for the treatment of various ailments. Any alteration to these medical records could result in a misdiagnosis that could lead to incorrect treatment or even death. Medical images include image metadata and information on the patient's medical history [1]. According to the medical imaging protocol, the image header contains a generic metadata format. A crucial aspect of medical diagnosis for patient monitoring is contingent upon the capacity of radiologists to conduct a reliable diagnosis based on the obtained images. The determination of the diagnosis is heavily dependent on a thorough visual examination of the morphology of the lesions. The implementation of user-friendly interfaces is of the utmost importance in facilitating accurate visual examination by radiologists and enabling the efficient identification of lesions [2,3]. The patient information, as well as the medical imaging and acquisition features, are all described in the metadata. This information is susceptible to being lost or changed; the images should be viewed with suspicion during transmission in electronic healthcare systems. A high level of privacy

and security is required whenever sensitive digital medical images are stored, shared, or transferred over a network. Throughout the transmission process, digital medical images are vulnerable to being accidentally distorted by signal processing techniques such as compression, noise, segmentation, etc. [4–7]. In the case of medical images, legitimacy is another important issue [8]. Therefore, it is important to put a lot of emphasis on legitimacy and integrity when sharing medical images [9–11]. Steganography [12], data encryption [13], and digital watermarking [14] are some examples of useful techniques to secure digital content. However, digital image watermarking provides efficient ways to protect and secure digital images from malicious or unintentional distortion as well as safeguard the confidentiality of patients [7,15,16].

Watermarking has been an important research topic for decades. It is one of the most widely used methods of protecting digital content. It is advisable to employ an invisible watermark that is indecipherable to human senses. Effective image watermarking systems must balance imperceptibility and robustness, register ownership information, and demonstrate dependability [17,18]. Robustness in watermarking means recognizing a watermark despite well-known attacks. A secure watermarking system should prevent detection, removal, and alteration [19]. Moreover, another important aspect of watermarking schemes is that they are imperceptible to the human visual system. In certain watermarking applications, however, slight distortions are acceptable in order to obtain higher robustness at a lower price [14,17]. In addition, security and payload are also regarded as important aspects when designing a watermarking scheme [20]. In the literature, there are several methods of image watermarking that were developed to meet the aforementioned objectives. A robust watermarking scheme should sustain itself against a wide range of attacks such as compression, filtering, noise addition, etc. Since Hessenberg decomposition offers remarkable features in image watermarking for the development of robust and secured watermarking schemes, Many researchers have used Hessenberg in their robust and secure watermarking schemes. Moreover, the transform domain is often used to improve the imperceptibility of a watermarking scheme. There are several reports available in the literature, such as [17,18,20–32].

Abdallah et al. [23] used non-negative matrix factorization and three-dimensional mesh spectra to develop a secure and robust watermarking scheme. The fundamental concept entails iteratively applying encryption to a watermark vector; then, the data are subsequently integrated into the spectral entries of a compact 3D mesh. This method requires the removal of the original object and is non-blind, but it is resistant to a variety of attacks. Su and Chen [22] presented blind, robust watermarking for spatial colour images. This approach separates the cover image into red, green, and blue (RGB) channels and embeds it in the blue channel. The process of embedding a binary watermark involves partitioning it into four sub-watermarks, and the blue channel pixel values are manipulated to embed the elements into the distinct areas of the cover image. The aforementioned task is achieved by employing the direct current coefficient and the primary characteristics of generation. The reconstruction or recovery of the watermark image is accomplished through the utilisation of DC coefficients, quantization based on a key, and various statistical principles and procedures. This approach was deemed secure due to its utilisation of encryption and confidential keys. Selesnick [24] presented a reliable discrete cosine transform (DCT)-based watermark for blind grayscale images. The method under consideration employs mixed modulations and a partially sign-altered mean in the utilisation of the discrete cosine transform, which facilitates the attainment of data balance and enables the embedding of multiple coefficients, thereby enhancing attack strength while maintaining a low bit error rate. The proposed scheme demonstrates enhanced resilience and visual excellence with an average of 40 dB. Furthermore, Wang et al. [33] presented a hybrid and resilient approach for embedding watermarks in colour images through the utilisation of Discrete Wavelet Transform (DWT) and LU decomposition. The proposed methodology involves an initial DWT-based transformation of the cover image. Subsequent to the initial stage, the Low-High (LH) and High-Low (HL) sub-bands are subjected to a process of selection and

separation, resulting in the formation of discrete and mutually exclusive blocks. The blocks are subjected to LU decomposition, following which the encrypted watermark image is incorporated into the upper triangular matrices of the blocks. The plan under consideration exhibits a significant degree of resilience. Moreover, Liu et al. [25] suggested using the Affine transformation and Schur decomposition to create a reliable blind colour image watermarking system. The upper triangular matrix of the Schur decomposition is used to quantify the diagonal eigenvalues after the watermark image has been encrypted using the Affine transformation. The suggested scheme has low computational requirements and good resistance to numerous attacks. Hsu and Hu [26] presented a reliable DCT-based watermark for blind grayscale images. The proposed method utilises advanced techniques to enhance the security of the data and increase its strength against potential attacks. The proposed scheme offers excellent robustness and imperceptibility with a low bit error rate and an average of 40 dB. Another study investigated two distinct applications utilising deep learning-based generative adversarial networks (GANs) and transfer learning for magnetic resonance imaging (MRI) reconstruction procedures for brain and knee imaging. The approach facilitates the implementation of forthcoming MRI reconstruction models, obviating the need for extensive imaging datasets [34–36].

Additionally, Kalra et al. [37] introduced a robust watermarking technique for colour images that utilised DWT and DCT transformations. The watermark image is well protected with multiple security-enhancing techniques before embedding. The embedding process involves the selection of the middle-frequency band, followed by the application of 8×8 blocking and DCT. This is applied to the cover image's two-level DWT decomposition's middle-frequency band. The cover image is now ready to undergo the two-level DWT process after being shrunk. By determining the location of the watermark pixel for non-overlapping 8×8 blocks using column and row numbers, we can successfully embed the watermark. Furthermore, the watermark is securely embedded within the chosen blocks using a sophisticated low-frequency technique. Balasamy and Ramakrishnan [27] proposed a novel watermarking scheme based on the wavelet transform and particle swarm optimization (PSO). In this scheme, the host image is transformed using wavelet transform, and the watermark is protected using a tent map and hash function. The scheme achieves high PSNR. Saxena and Mishra [21] used a variant of multi-objective-PSO to develop a watermarking scheme. The primary objective of this scheme is to select the leader with the shortest distance from the region that the particle has recently visited. Sisaudia and Vishwakarma [28] proposed a kernel extreme learning machine and PSO-based watermarking scheme to secure watermarks. The PSO is used to optimize the scaling factor for the watermarking process. The scheme achieves high PSNR values for the watermarked images. Ali and Ahn [38] presented DWT-singular value decomposition (SVD)-based self-adaptive differential evolution-based watermarking scheme in which multiple scaling factors are optimized to embed imperceptible watermarks. Kazemivash and Moghaddam [39] has developed a robust and secure watermarking model by combining the regression tree and firefly algorithms to optimize scaling factors. Moeinaddini [40] presented a watermarking scheme to balance imperceptibility and robustness by combining entropy and a distinct discrete firefly algorithm for optimization. Using the Bat optimization algorithm, Pourhadi and Mahdavi [41] presented a robust and optimized digital image watermarking scheme based on the stationary wavelet transform to correct the geometric attack. Rajpal et al. [42] proposed a watermarking scheme to optimize multiple scaling factors using online sequential extreme learning machine. Sharma and Mir [43] used the meta-heuristic optimization approach to develop an optimized watermarking scheme. Idowu et al. proposed a framework-based statistical and morphological model that is capable of effectively executing concurrent denoising and enhancement procedures. The aim of this study was to devise a maximum a posteriori (MAP) estimator for the coefficient that is free from any noise. The utilisation of a statistical model eliminates the need for the estimation of the noise level and enables the model to automatically adapt to the observed image data.

The methodology was devised with the aim of preserving the genuineness of the image's delicate characteristics [44].

To obtain a more robust and secure watermarking scheme, the majority of the aforementioned studies have shifted from traditional watermarking to either heuristic-search-based or nature-inspired watermarking techniques. Although many decomposition-based watermarking schemes exist, their efficacy is inferior. PSO has been used in a variety of research and application domains in recent years. PSO has gained widespread attention in recent years due to its ease of implementation and rapid convergence to acceptable solutions. Although the PSO method has been used to solve search and optimization problems, it is susceptible to becoming trapped in local optima. Therefore, the proposed technique combines the lifting wavelet transform (LWT) and the Hessenberg decomposition and approaches for nature-inspired optimization for watermark embedding. Extensive tests show that our proposed method outperforms previous approaches. The suggested optimal watermarking scheme provides better robustness. The major contributions of the proposed scheme are as follows:

- The utilisation of the two-level transform LWT was employed to achieve the robustness of watermarked ultrasound medical images.
- The use of the Arnold transform enhances the security of watermarked images.
- The Hessenberg decomposition is employed to attain a high level of imperceptibility in watermarked images.
- The PSO technique was employed to determine the optimal value of the multi-valued scaling factor in the proposed watermarking methodology.

The rest of the paper is organized as follows: Section 2 provides an overview of the techniques we use and provides context for the conversation that follows. Section 3 explains the suggested research approach for watermark embedding and extraction. Section 4 discusses the results. Section 5 concludes our work.

2. Preliminaries

The lifting wavelet transform (LWT) and particle swarm optimization used in our work are briefly explained in this section.

2.1. Overview: Particle Swarm Optimization

Particle swarm optimization (PSO) is a technique for iterative optimization inspired by nature that was developed by Eberhart and Kennedy in 1995 [45] (as in Algorithm 1). It is comparable to a flock of birds seeking food, with each bird representing a particle. This collection of particles makes up a swarm. The procedure commences with the random initialization of swarm particles. Each particle's position and velocity are distinct. In other words, a particle swarm is a collection of potential solutions to the optimization problem that may flow in the search parameter space as trajectories are based on the optimal performance of itself and its neighbours. The PSO can be used to both maximize and minimize problem occurrences. The optimal particle is identified using a fitness function or objective function, and all particles modify their velocities and locations to migrate toward the optimal particle. The particle that is farthest from the optimal solution modifies its maximal velocity to approach it. This procedure continues until the requisite solution is attained or the termination criteria are met. PSO is well liked because its implementation is less complicated than that of other optimization strategies. Figure 1 depicts the process flow of the watermarking scheme.

```

1 Algorithm 1. Particle Swarm Optimization
2 Input: Embedding Algorithm, Extraction Algorithm, Number of Iteration,
   Population, Number of Attacks, Names of Attack, Fitness Function, Cover
   Image, Watermark, Iteration.
3 Output: Robust Watermarked Image.
4 BEGIN:
5   Initialize Swarm Population
6   Initialize fitness value
7   for i = 1 to Iteration
8     WatermarkedImage = Embed Watermark using Embedding Algorithm 2
9     Perform Image Processing Attacks on WatermarkedImage
10    Get Extracted Watermark Using Extraction Algorithm 3
11    Calculate New Fitness Value
12    end if Optimum Solution Achieved
13    else loop
14  end for
15  return Watermarked Image
16 END:

```

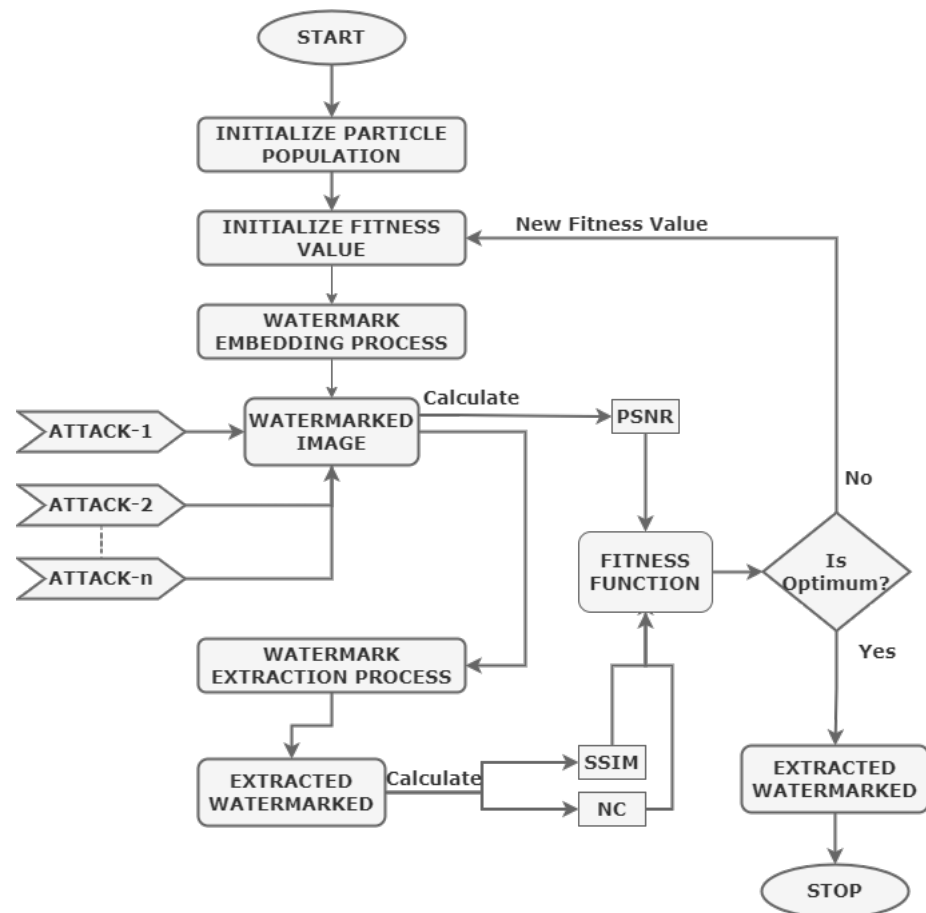


Figure 1. Flowchart: Particle Swarm Optimization for Watermarking Scheme.

2.2. Lifting Wavelet Transform

In order to generate bi-orthogonal wavelets, a novel method known as the lifting wavelet transform (LWT) was developed. A flaw of the conventional discrete wavelet transform resulted in the development of LWT. The direct evaluation in the integer domain is used in this approach, which greatly simplifies the solution to the reversibility problem. Since LWT is superior to DWT in time and space, it is widely employed in the image-processing industry. If the lifting process is changed, this technique can produce wavelets from a second generation. Because it uses an in-place realization technique for the wavelet transform, the lifting wavelets technique can significantly reduce the processing time and

memory requirements [46]. It outperforms DWT in terms of time and space; as a result, it may find extensive use in image processing [47]. The signal is split into its component parts across three stages during the LWT process: split, predict, and update, as shown below.

- **Split:** Separate, non-overlapping sets of odd and even samples of the signal $\Phi(n)$, calculated using Equation (1).

$$\Phi_e = \Phi(2n) \text{ and } \Phi_o = \Phi(2n + 1) \tag{1}$$

- **Predict:** By abstracting the difference, the split samples can be utilised to forecast each other if they are associated. The values predicted can be calculated using Equation (2).

$$\Psi(n) = \Phi_o(n) - Y[\Phi_e(n)] \tag{2}$$

where $Y[\Phi_e(n)]$ and $\Psi(n)$ are the predict operator and high-frequency components, respectively, which are used to describe the difference between the original sample value and the anticipated value [48].

- **Update:** After updating the even samples $\Phi_e(n)$ with the update operator $Updt(n)$, the low-frequency component $lfc(n)$ is represented by the abstract difference $\Psi(n)$, which is a rough approximation of the original signal $\Phi(n)$ defined in the following Equation (3) [48].

$$lfc(n) = \Phi_e(n) + Updt(G(n)) \tag{3}$$

2.3. Hessenberg Decomposition

The process of decomposing a general matrix X into orthogonal similarity transformations can be achieved through the utilisation of Hessenberg decomposition, as stated in reference [49] and represented by Equation (4).

$$X = QHQ^T \tag{4}$$

If $i > j + 1$, then h_{ij} is equal to zero. This is due to the fact that matrix Q is orthogonal and matrix H is an upper Hessenberg matrix, which renders them incompatible with each other. Typically, the Hessenberg decomposition is obtained through the utilisation of a householder matrix (ρ). The householder matrix can be categorized as an orthogonal matrix.

$$\rho = \frac{I_n - 2uu^T}{u^T u} \tag{5}$$

The variable u in the equation for ρ_n represents a non-zero vector, while I_n denotes an identity matrix with dimensions of $n \times n$. When the size of matrix A is $n \times n$, the entire process consists of $n - 2$ steps. The Equation (6) is utilised for the computation of Hessenberg decomposition.

$$\begin{aligned} H &= (\rho_1, \rho_2, \dots, \rho_{(n-3)}, \rho_{(n-2)})^T A (\rho_1, \rho_2, \dots, \rho_{(n-3)}, \rho_{(n-2)}) \\ H &= Q^T A Q \\ A &= QHQ^T \end{aligned} \tag{6}$$

The proposed watermarking method employs both the Hessenberg decomposition and the LWT. The suggested technique for watermarking exhibits imperceptibility to the human visual system and resilience to a diverse range of attacks. The Hessenberg decomposition is utilised to transform a generic matrix A into orthogonal similarity transformations. Colour images are composed of individual colour channels, each of which consists of a grayscale value ranging from 0 to 255. The orthogonal matrix exhibits minimal alteration if and only if the Hessenberg decomposition is employed to embed the pixel block. Upon examining a unitary matrix, it was observed that the elements in the succeeding column bear a striking resemblance to those in the preceding column. So, no two components of Q are identical to one another. Modifying the adjacent column has the potential to render the watermark

indiscernible. The recommended approach combines FRT and Hessenberg embedding to achieve strong watermarking and a large payload. The watermark must be encoded so that it can be extracted from the image even if the image processing pipeline has been compromised. The use of frequency-domain modifications in image watermarking is, therefore, very common.

2.4. Arnold Transform

Arnold transform (AT) is mostly used for scrambling. It is used in image processing to jumble the location of pixels in order to save storage space [50]. A square matrix of $N \times N$ and coordinates are $K = \{(\alpha, \beta) | \alpha, \beta = 0, 1, 2, \dots, N - 1\}$. The AT can be expressed as follows:

$$\begin{pmatrix} \alpha_n \\ \beta_n \end{pmatrix} = \begin{pmatrix} 1 & a \\ \beta & a\beta + 1 \end{pmatrix} \begin{pmatrix} \alpha_{n-1} \\ \beta_{n-1} \end{pmatrix} \text{mod } N \tag{7}$$

The coordinates α_n and β_n are utilised to transform with regard to $\alpha_{(n-1)}$ and $\beta_{(n-1)}$ after m iterations, respectively, a and b are positive values, and N is the width and height of a square matrix. When (α, β) is modified numerous times, the AT is iterative. It reverts to its former state.

2.5. Performance Metrics

It is possible to provide a numerical value for the degree to which the cover image and the watermarked image differ from each other. The quality of the original cover image is diminished when it is watermarked or otherwise altered. As a result, evaluating its quality is essential [51]. When a cover image is watermarked or altered in another way, its quality is diminished. Therefore, assessing its calibre is imperative. By utilising the peak signal-to-noise ratio (PSNR) formula as shown in Equation (8), it becomes feasible to evaluate the degree of resemblance between the watermarked image and the original image. The PSNR scale is expressed in decibels (dB). A greater PSNR indicates a higher degree of similarity between the unaltered and watermarked versions of the image.

$$\text{PSNR} = 10 \times \log_{10} \left(\frac{255^2}{\text{MSE}} \right) \tag{8}$$

The error can also be quantified by comparing the original and watermarked versions of an image using a metric called mean squared error (MSE). The MSE can be computed using Equation (9), where C represents the original, unmodified image, and CW represents the modified, watermarked version.

$$\text{MSE} = \frac{1}{M \times N} \sum_{x=0}^{M-1} \sum_{y=0}^{N-1} (C(x, y) - CW(x, y))^2 \tag{9}$$

A comprehensive evaluation of the watermark retrieval quality is necessary to effectively evaluate the efficacy of the watermarking system. When evaluating the reliability of a watermarking system, academics typically use both the normalized correlation (NC) and the structural similarity index measure (SSIM) [52]. While SSIM analyses the structural similarities between the two images, the degree of similarity within the original and watermarked copies is assessed by NC. The NC and SSIM can be obtained by solving their respective equations, denoted as (10) and (11).

$$\text{NC} = \frac{\sum_{x=1}^M \sum_{y=1}^N w(x, y) \times w'(x, y)}{\sum_{x=1}^M \sum_{y=1}^N w^2(x, y)} \tag{10}$$

To distinguish between the original watermarked image (w) and the recovered watermarked image (iw'), we use the symbols i and w' , respectively.

$$SSIM = \frac{(2\mu_w\mu_{w'} + C_1)(2\sigma_{ww'} + C_2)}{(\mu_w^2 + \mu_{w'}^2 + C_1)(\sigma_w^2 + \sigma_{w'}^2 + C_1)} \tag{11}$$

3. Proposed Technique

This section discusses the proposed technique for medical image watermarking, which is designed to be imperceptible to the human eye. In order to satisfy the criteria for image security and robustness of a watermarked image, a binary watermark image is inserted into the green channel of a medical image with colour. The scheme that has been put forward is explicated in Sections 3.1 and 3.2, correspondingly. Section 3.3 provides an explanation of the parameter settings and application of the proposed enhanced particle swarm optimization (PSO) algorithms for the purpose of determining suitable scaling factors.

3.1. Watermark Embedding Process

In this subsection, we discussed the procedure for embedding a watermark (illustrated by the Figure 2). The method for embedding the watermark is given in Algorithm 2. The watermark embedding algorithms take two inputs viz a colour medical image (called the host image) and a binary watermark. In the first stage, the host image is separated from its colour components (R, G, B). In the second stage, the green channel of the host image is transformed using LWT to acquire the low-frequency sub-bands (i.e., LL, LH, HL, HH). In the third stage, low-frequency sub-bands (LL) are converted into 3×3 block. As shown in Figure 3, the blocks are chosen in a zigzag pattern. In the fourth stage, each block is decomposed using the Hessenberg decomposition to obtain the Q matrix. In the fifth stage, the Arnold cat map encryption method is used to encrypt the watermark bits. In the sixth stage, the marking bits are multiplied with Δ and added to the central element of Q matrix to obtain the Q' matrix. Here, the value of Δ is optimized by the PSO algorithm. The range of Δ is between 0.020 and 0.040. In the seventh stage, modified blocks are obtained via inverse Hessenberg decomposition. In the eighth stage, the modified blocks are rearranged into the LL sub-band. In the ninth stage, the H'_g modified green channel of the host image is transformed using inverse LWT. Finally, all colour channels are combined to produce the watermarked image.

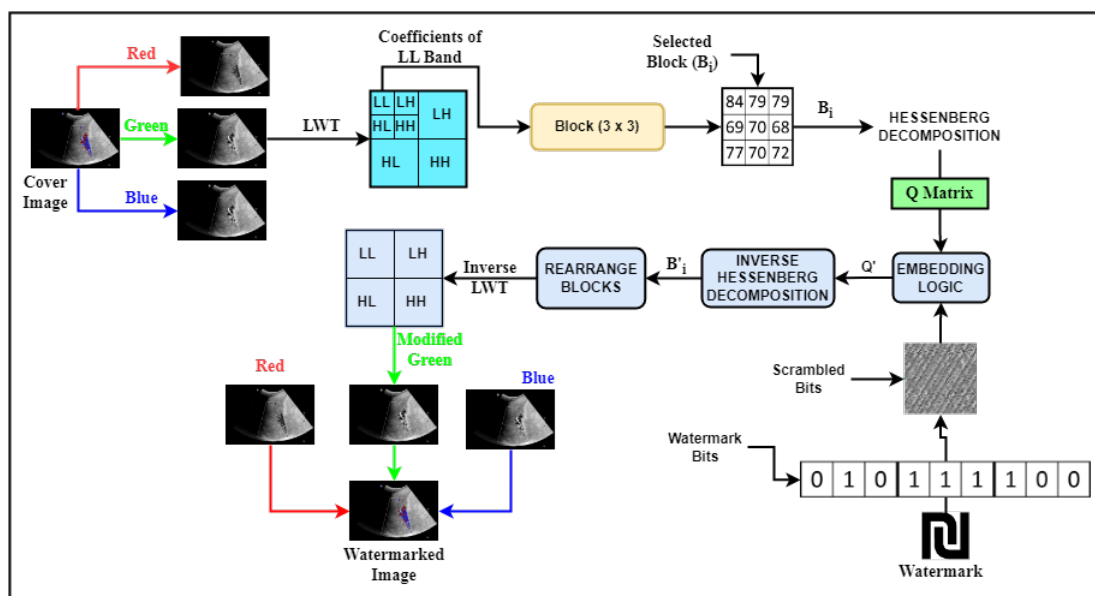


Figure 2. Block Diagram: Watermark Embedding Process.

```

1 Algorithm 2. Watermark Embedding process
2 Input: Host Image (Colour Medical Image) as  $H$  and a binary watermark ( $W$ )
3 Output: Watermarked image  $H'$ 
4 BEGIN:
5    $[H_r, H_g, H_b] = [\text{red}(H), \text{green}(H), \text{blue}(H)]$ 
6    $[LL, LH, HL, HH] = \text{Iwt}(H_g)$ 
7    $b_i = \text{getBlock}(LL, \text{blockNumber})$ 
8    $[Q, H, Q^T] = \text{Hberg}(b_i)$ 
9    $\text{encrypted} = w\_image \oplus k$ 
10   $Q' = Q + \Delta * W_i$ 
11   $b'_i = \text{IHberg}(Q', H, Q^T)$ 
12   $LL' = \text{setBlocks}(LL, b'_i, \text{blocksNumber})$ 
13   $H'_g = \text{ilwt}(LL', LH, HL, HH)$ 
14   $H' = [H'_g, H_g, H_b]$ 
15  Obtained watermarked image ( $H'$ )
16 END

```

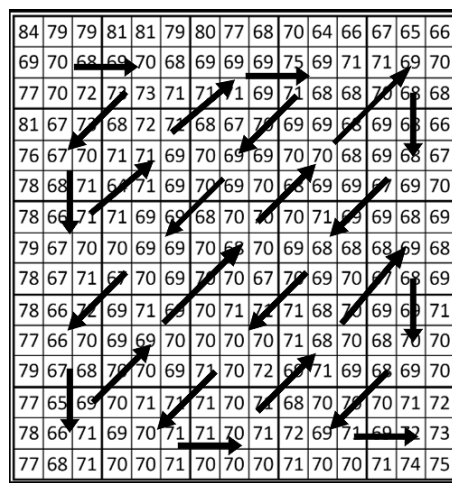


Figure 3. Zig-Zag Block Selection Diagram.

3.2. Watermark Extraction Process

The following section outlines the methodology employed for the extraction of watermarks. The process of extracting the watermark is illustrated in Figure 4. The technique for incorporating the watermark is described in detail in Algorithm 3 which takes the colour medical image (H') as an input and returns the extracted watermark. In the first stage, the watermarked image's colour channels are separated into red, green, and blue. In the second stage, the extracted green channel of the watermarked image is transformed using the LWT transform to acquire low-frequency sub-bands (LL). In the third stage, the low-frequency sub-band is divided into 3×3 blocks. Each of these blocks is chosen in a zigzag pattern. In the fourth stage, Hessenberg decomposition is used to acquire the Q matrix containing the watermark bits. In the sixth phase, the watermark bits are extracted. In the sixth stage, the extracted watermark is obtained by scrambling the watermark bits .

```

1 Algorithm 3. Watermark Extraction Process
2 Input: Watermarked Colour Medical Image ( $H'$ )
3 Output: Extracted Watermark
4 BEGIN:
5    $[H'_r, H'_g, H'_b] = [\text{red}(H'), \text{green}(H'), \text{blue}(H')]$ 
6    $[LL', LH', HL', HH'] = \text{Iwt}(H'_g)$ 
7    $b'_i = \text{getBlock}(LL', \text{blockNumber})$ 
8    $[Q', H, Q^T] = \text{Hberg}(b'_i)$ 
9    $W' = \begin{cases} 1, & \text{if } Q' + \Delta \leq \lambda \\ 0, & \text{Otherwise} \end{cases}$ 
10   $W'' = W' \oplus k$ 
11  Obtain extracted watermark as ( $W''$ )
12 END

```

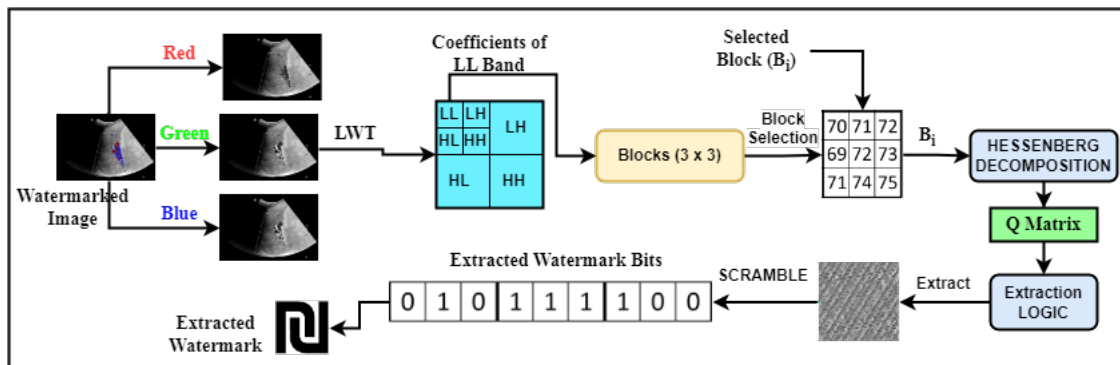


Figure 4. Block Diagram: Watermark Extraction Process.

3.3. Role of PSO in Finding Optimal Scaling Factor

The efficiency of watermarking is influenced by a number of characteristics, with imperceptibility and robustness being two of the most crucial. On the contrary, these two concepts are irreconcilable. Therefore, it is important to examine the trade-off between robustness and imperceptibility while developing a watermarking scheme [45]. PSO has some natural advantages over other intelligent optimization algorithms, such as theoretical simplicity, a lower number of parameters to adjust, and the ability to escape the local optimal condition through the integration of local and global information, particularly in multidimensional and nonlinear situations. These appealing qualities have contributed to the widespread use of PSO. In recent years, the PSO method has been successfully used to solve search and optimization problems. It has been demonstrated that PSO can achieve better optimization solutions in a faster and less expensive manner than many other methods. As a result, it can efficiently identify the optimal global (or near globally optimum) solution in multidimensional search spaces. This is a primary reason for utilising PSO at work. Furthermore, the classic PSO algorithm's global convergence cannot always be ensured because swarm diversity decreases as evolution progresses. To address this issue, this research employs a multi-objective PSO variation to reduce flaws. Since the majority of multi-objective PSO variant algorithms [53,54] utilise an external archive to preserve a collection of Pareto optimal solutions that approximate the actual Pareto front. Certain variations of multi-objective PSO [55] operate under the assumption of an infinite archive size, whereas the majority of other variants employ a fixed archive size. The exponential increase in non-dominated solutions for multi-objective PSO algorithms results in a significant expense when updating the archive set, should an unlimited archive size be employed. Therefore, it cannot be deemed a cost-effective solution for archive maintenance. In the case of an archive with a fixed size, it is necessary to establish regulations for managing instances of overflow within the archive. The regulations in question serve to screen the archive, utilising specific criteria, including density [56], in order to maintain the archive's size below the maximum permissible limit. In cases where the archive has reached maximum capacity, the superior solution, as determined by the designated metric, supplants the archive member with the lowest assigned value. The guidance mechanism plays a crucial role in the identification of optimal solutions by determining the trajectory of particles within the search space. Particles are provided with direction through the utilisation of the global best (gbest) and personal best (pbest). The performance of gbest is contingent upon the imperceptibility of the watermarked images, whereas pbest is contingent upon the structural similarity index (SSIM) and normalized correlation (NC) of the extracted watermark following a series of image processing attacks. In order to reduce the trade-off between robustness and imperceptibility, a fitness function based on PSNR, SSIM, and NC was derived in Equation (12).

$$fitness = |PSNR - \Delta| + \left[\left(1 - \frac{1}{N} \sum_{i=1}^N \alpha_i \right) + \left(1 - \frac{1}{N} \sum_{i=1}^N \beta_i \right) \right] \quad (12)$$

where N is the number of attacks, α and β is NC and $SSIM$ values of extracted watermark, respectively, and Δ is the optimization parameter to guarantee the optimum imperceptibility of the watermarked image.

4. Simulation Results and Discussion

This section examines the anticipated work and discusses the results. Various types of colour ultrasound images and binary watermark images have been used to test how well the method works. The proposed work was simulated using MATLAB R2015a on a Windows 11 machine with 16 GB of RAM and a core i7 processor. This allowed us to assess the effectiveness of the proposed technique in terms of imperceptibility and robustness. The selected cover medical image has dimensions of 1024×768 pixels, sourced from The National Library of Medicine image database (<https://medpix.nlm.nih.gov>, accessed on 12 April 2023). Additionally, the binary watermark has dimensions of 64×64 pixels. Figure 5 depicts the test medical images as well as the watermark.

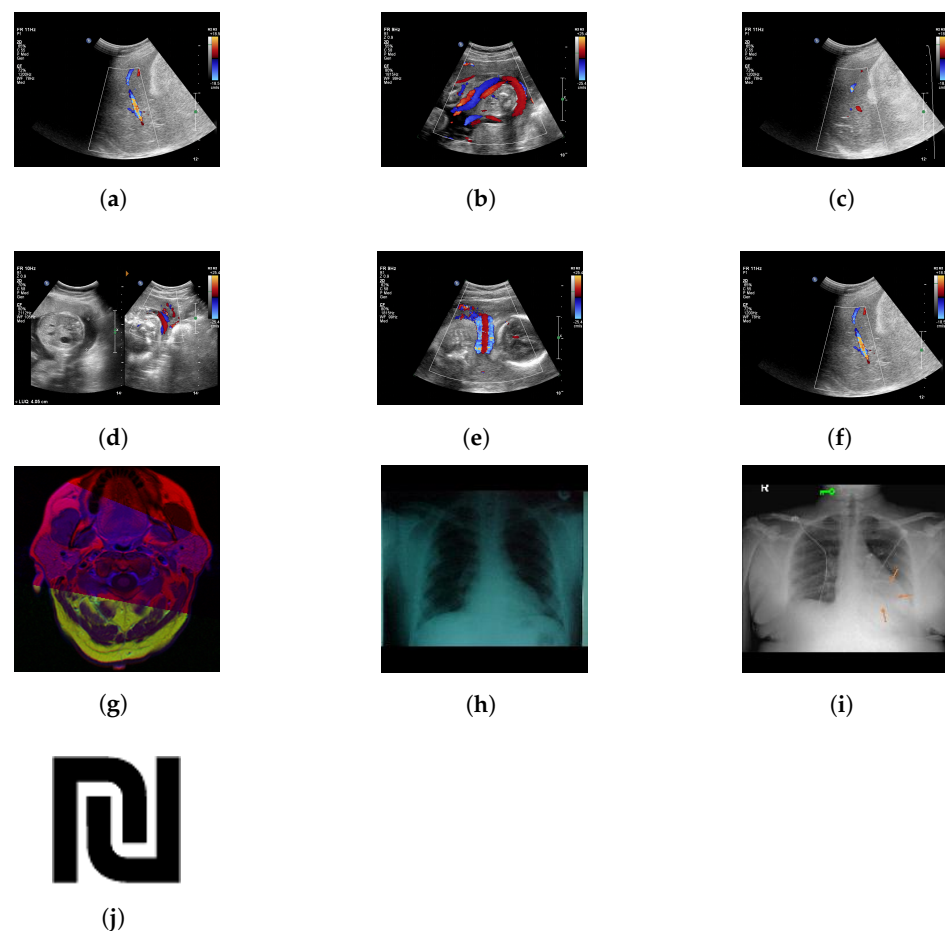


Figure 5. Test set: Colour medical image and binary watermark.

Figure 6 shows the watermarked image and the retrieved watermark. It shows that the proposed watermark embedding and extraction technique works well. Each experimental image's caption includes the PSNR value of the watermarked image. The normalized cross co-relation values are also displayed as the captions for the retrieved watermark images. Table 1 displays the PSNR and SSIM values of the watermarked images, along with the NC and $SSIM$ values of the extracted watermark. The maximum peak signal-to-noise ratio (PSNR) and structural similarity index (SSIM) values achieved are 55.9115 and 0.9898, respectively. The watermarked image effectively showcases the robust imperceptibility of the watermark. Moreover, the technique for extracting watermarks is efficacious. The proximity of the NC and $SSIM$ values to unity is indicative of the proficient performance of the extraction algorithm.

Table 1. PSNR of different types of colour medical images and SSIM and NC of the extracted watermark without attack.

Image	(a)	(b)	(c)	(d)	(e)	(f)	(g)	(h)	(i)
PSNR	59.24	59.38	59.07	59.18	59.55	59.43	59.21	59.34	59.38
Average PSNR	59.308								
NC	1.0000	1.0000	1.0000	1.0000	1.0000	1.0000	1.0000	1.0000	1.0000
SSIM	0.9987	0.9991	0.9983	0.9988	0.9995	0.9992	0.9993	0.9991	0.9991

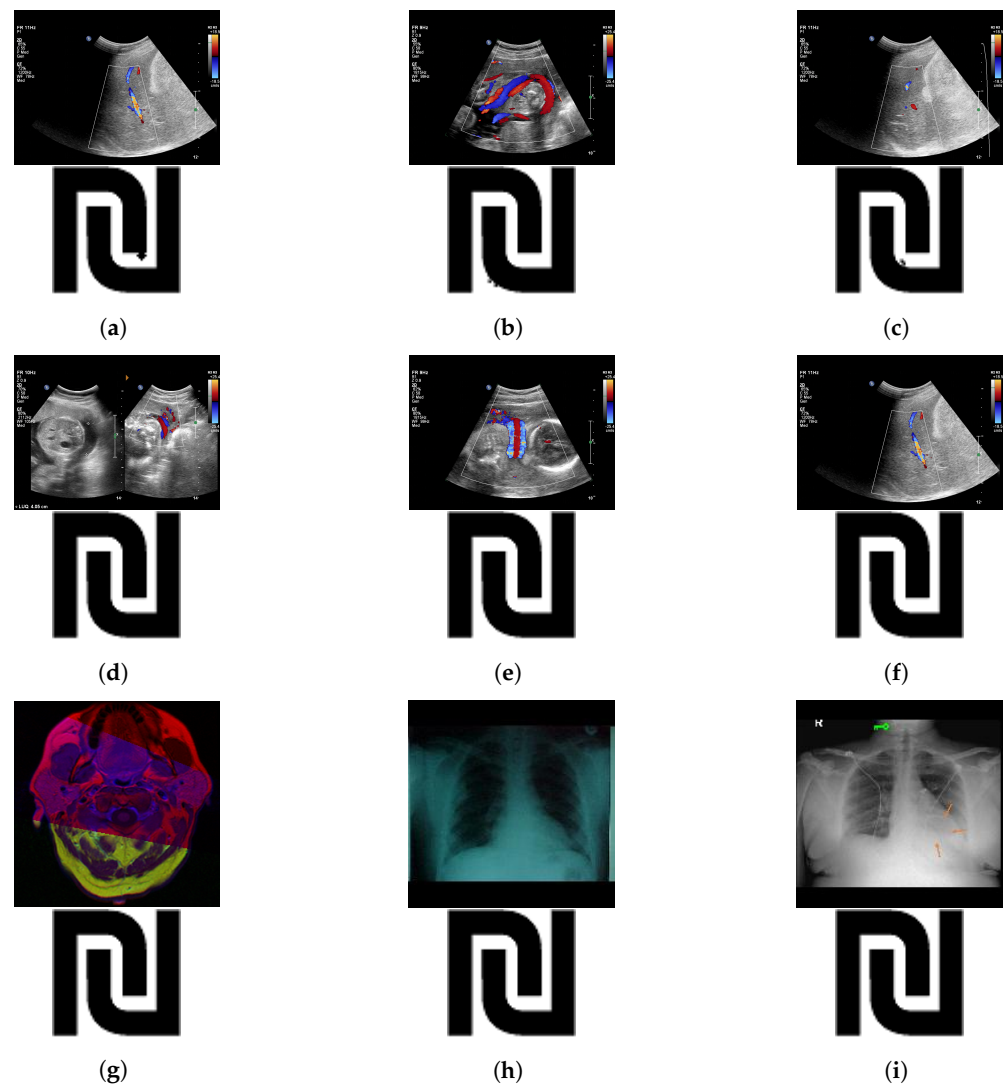


Figure 6. No Attack: Watermarked Image and Extracted Watermark.

4.1. Robustness Results Evaluation

The efficacy of the watermarking methodology has been evaluated across various image processing benchmarks. The watermarked image undergoes the interpolation of image processing attacks, including but not limited to filtering, compression, and noise. Subsequently, the watermark is restored. The evaluation of a watermarking system’s resilience is conducted through the computation of the NC and SSIM metrics for the recovered watermark. This section presents a review of the results obtained from various image-processing attacks.

4.1.1. JPEG Compression

Amidst the COVID-19 pandemic, patients were diagnosed utilising a remote approach. Medical images are frequently transmitted through diverse communication channels. The medical images were either purposefully or accidentally compressed and transformed throughout this procedure. The quality of converted medical images is always lower than the original. Consequently, JPEG compression has rapidly become an established and indispensable tool in the field of image processing. We examined extracted watermark images with various quality parameters scale (from 40 to 90) in Figure 7. The NC and SSIM values that were obtained through the course of our investigation are presented in Table 2. The NC values range from 0.9634 to 1.0 for quality factors 40–90. However, the obtained SSIM values range from 0.8642 to 0.9712 for quality factors 40–90. The obtained results demonstrate that, when exposed to a JPEG compression attack, the proposed approach performed better than expected.

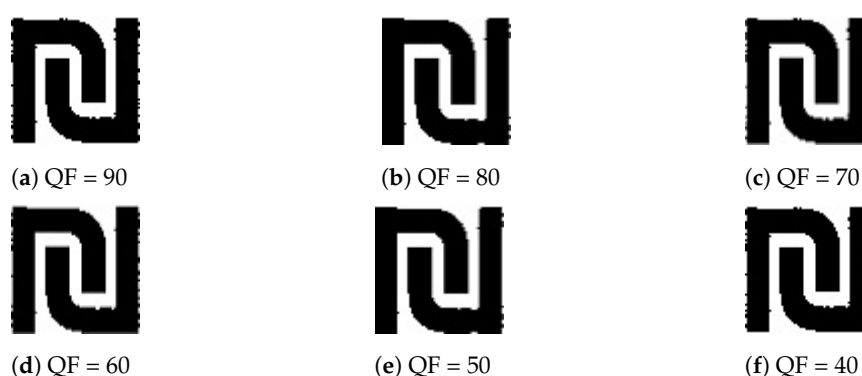


Figure 7. Extracted watermark after JPEG compression attacks with different quality factors.

Table 2. JPEG Compression: NC and SSIM of Extracted Watermark.

Quality Parameter	NC	SSIM
90	1	0.9712
80	0.9985	0.9611
70	0.9943	0.9523
60	0.9823	0.9383
50	0.9774	0.8976
40	0.9634	0.8642

Furthermore, upon conducting a comparative analysis of the outcomes with other pre-existing methodologies, namely [28,30–32], concerning quality factors 80 and 90 (as presented in Table 3), it was observed that the outcomes of [28,32] exhibit a resemblance to the proposed scheme at a quality factor of 90. At a quality factor of 80, it can be observed that only the reference [32] is in closer proximity to the subject matter being discussed. Thus, it can be inferred that the proposed methodology exhibited superior performance in comparison to various analogous methodologies.

Table 3. Comparison of NC Values over JPEG Compression Attack.

QF	Proposed Work	[28]	[31]	[30]	[32]
90	1.0000	1.0000	0.9941	0.9901	1.0000
80	0.9985	0.9781	0.9897	0.9813	0.9945

4.1.2. Filtering Attack

The images are distorted by the communication channel signals. The watermark image is also subject to interpolation attacks involving distortion or signal processing. This presents a novel prospect to acquire knowledge on image processing methodologies,

including the filter attack technique. The performance of the proposed watermarking scheme was effectively evaluated in our experiment, specifically in the context of a filtering attack. The results depicted in Figure 8 indicate that the extraction of the watermark image from the distorted watermarked image remains feasible despite the presence of a filtering attack. The aforementioned outcome exhibits the durability of the watermarking methodology, thus holding potential for further development. The results of our experiment are presented in Table 4, which provides a valuable foundation for subsequent analysis. The findings indicate that the envisaged system exhibited satisfactory performance, even in the presence of a filtering attack.

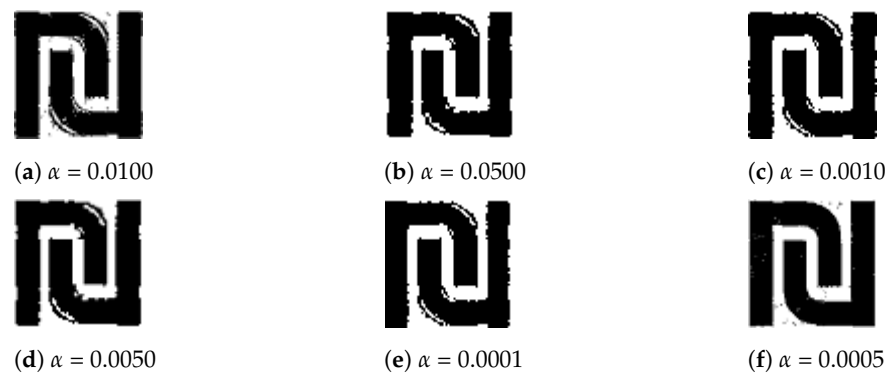


Figure 8. Extracted Watermark after Filtering Attack.

Table 4. Filtering Attack: NC and SSIM of Extracted Watermark.

α	NC	SSIM
0.0500	0.7211	0.7332
0.0250	0.7713	0.7881
0.0100	0.8213	0.8551
0.0050	0.8479	0.8643
0.0020	0.9331	0.8997
0.0010	1.0000	0.9887

Furthermore, upon conducting a comparative analysis of the outcomes with other extant methodologies, namely [28,30–32], at intensities of 0.05, 0.025, and 0.10 (as presented in Table 5), it was noted that the findings of [31,32] bear similarity to the suggested approach at an intensity of 0.050. At the intensity of 0.025 and 0.010, the performance of our approach is much better than other similar schemes. Thus, it can be inferred that the proposed methodology exhibited superior performance compared to various analogous methodologies.

Table 5. Comparison of NC value on Filter Attack.

α	Proposed Work	[28]	[31]	[30]	[32]
0.0500	0.7211	0.6331	0.7089	0.6811	0.7298
0.0250	0.7713	0.6597	0.7221	0.7212	0.7399
0.0100	0.8213	0.7712	0.7689	0.7551	0.7611

4.1.3. Noise Addition Attack

The susceptibility of the proposed scheme to noise interference on the watermarked image has been assessed. Different levels of noise, ranging from 0.001 to 0.020, were applied to the watermarked image. Subsequently, the watermark was extracted from the distorted image, as illustrated in Figure 9. As depicted in Figure 9, the extraction of the watermark from a distorted watermarked image is feasible even in the presence of a noise attack. The aforementioned outcome exhibits the durability of the watermarking methodology,

indicating potential for future applications. Table 6 displays the outcomes of watermark extraction from an image that has been watermarked and exposed to different levels of noise. The NC values corresponding to the intensity levels of 0.020, 0.010, 0.005, and 0.001 are 0.9715, 0.9791, 1.0000, and 1.0000, respectively. The SSIM values for intensity levels of 0.020, 0.010, 0.005, and 0.001 are reported as 0.8971, 0.9001, 0.9881, and 0.9891, respectively. The attained NC and SSIM values in our experiment serve as a promising foundation for subsequent analysis. The findings indicate that the envisaged system exhibited satisfactory performance even in the presence of a noise attack.

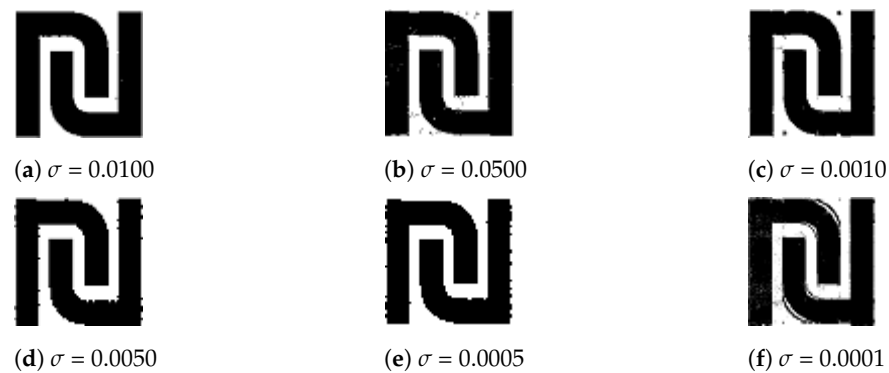


Figure 9. Extracted Watermark after Noise Attack.

Table 6. Noise Attack with Different Intensity: NC and SSIM of Extracted Watermark.

α	NC	SSIM
0.001	1.0000	0.9891
0.005	1.0000	0.9881
0.010	0.9791	0.9001
0.020	0.9715	0.8971

In addition, a comparative analysis was performed to evaluate the results of the proposed methodology in relation to other established approaches, specifically [28,30–32], with respect to varying noise intensity levels of 0.001, 0.005, 0.010, and 0.020 (as presented in Table 7). The findings indicate that the outcomes of [28,30] bear a resemblance to the proposed scheme at intensity levels of 0.001 and 0.020. At an intensity level of 0.010, it is apparent that [30–32] exhibit superior performance. However, the performance of intensity level 0.005 surpasses that of [28,30–32]. Therefore, it can be deduced that the suggested approach demonstrated better results when compared to several similar approaches.

Table 7. Noise Attack: Comparison of NC Values with Existing Schemes.

α	Proposed Work	[28]	[31]	[30]	[32]
0.001	1.0000	0.9991	0.9893	0.9997	0.9988
0.005	1.0000	0.9989	0.9901	0.9988	0.9981
0.010	0.9791	0.9785	0.9888	0.9818	0.9881
0.020	0.9715	0.9701	0.9725	0.9713	0.9711

4.1.4. Histogram Equalization Attack

Table 8 shows the histogram equalization attack on the watermarked image. Based on the preceding discourse, the benefits of the suggested plan are outlined as follows:

1. The proposed scheme’s PSNR is higher than that of other existing systems, demonstrating that the watermarked image quality is suitable for diagnosis.
2. The robustness of the proposed scheme is found better with similar existing schemes in various cases. However, in some attacks, its performance is quite similar.

3. The security of the embedded watermark is increased using the Arnold transform.

Table 8. Histogram Equalization Attack: NC and SSIM of Extracted Watermark.

α	NC	SSIM
0.001	1.0000	0.9891
0.005	1.0000	0.9881
0.010	0.9791	0.9001
0.020	0.9715	0.8971

5. Conclusions

The power of PSO optimization in combination with the LWT and Hessenberg decomposition, a new blind image watermarking method, has been proposed. It is based on image segmentation and the Arnold cat map. A number of tests were performed on the system to determine its stability, and the findings are compared to those of other similar schemes. The suggested method generated watermarked images with PSNRs between 59.07 and 59.43 when compared to previous schemes. Despite significant distortions caused by JPEG compression, additive noise, median filtering, or average filtering, the watermark can still be extracted from the image. The removal of the watermark from a compressed watermark image results in an increase in perceived quality. The NC value of the retrieved watermark shows how good it looks. Based on the results of the experiments, our suggested method does a better job of reducing distortion than the best methods that are currently being used. The watermarking technique presented in this study yields superior image quality as measured by PSNR, SSIM, and NC metrics, thus rendering it a viable option for medical image applications.

Author Contributions: Methodology, L.K.; Validation, K.U.S.; Formal analysis, I.K. and A.K.; Data curation, T.S.; Writing—original draft, L.K. All authors have read and agreed to the published version of the manuscript.

Funding: This research received no external funding.

Institutional Review Board Statement: For this study not involving humans or animals.

Informed Consent Statement: Not applicable.

Data Availability Statement: Medical images used in this study were taken from an open database available at (<https://medpix.nlm.nih.gov>, accessed on 12 April 2023).

Conflicts of Interest: The authors declare that there are no conflict of interest.

Abbreviations

The following abbreviations are used in this manuscript:

SVD	Singular Value Decomposition
SLT	Slantlet Transform
RSVD	Randomized Singular Value Decomposition
FA	Firefly Algorithm
MRI	Magnetic Resonance Imaging
CT	Computed Tomography
DICOM	Digital Imaging and Communications in Medicine
JPEG	Joint Photographic Experts Group
SSIM	Structural Similarity Index Metric
PSNR	Peak Signal-to-Noise Ratio
NC	Normalized Correlation
NIA	Nature Inspired Algorithm
MSF	Multi-valued Scaling Factor
SSF	Single-valued Scaling Factor
LWT	Lifting Wavelet Transform
IWT	Integer Wavelet Transform
PSO	Particle Swarm Optimization

MRI	Magnetic Resonance Imaging
GA	Genetic Algorithm
ABC	Artificial Bee Colony Algorithm
DWT	Discrete Wavelet Transform
MAC	Media Access Control
HD	Hessenberg Decomposition
LWT	Lifting Wavelet Transform

References

- Pianykh, O.S. *Digital Imaging and Communications in Medicine (DICOM): A Practical Introduction and Survival Guide*, 1st ed.; Springer Publishing Company, Incorporated: Berlin/Heidelberg, Germany, 2010.
- Calisto, F.M.; Ferreira, A.; Nascimento, J.C.; Gonçalves, D. Towards Touch-Based Medical Image Diagnosis Annotation. In Proceedings of the ISS '17: 2017 ACM International Conference on Interactive Surfaces and Spaces, Brighton, UK, 17–20 October 2017; Association for Computing Machinery: New York, NY, USA, 2017; pp. 390–395. [\[CrossRef\]](#)
- Dontchos, B.N.; Yala, A.; Barzilay, R.; Xiang, J.; Lehman, C.D. External validation of a deep learning model for predicting mammographic breast density in routine clinical practice. *Acad. Radiol.* **2021**, *28*, 475–480. [\[CrossRef\]](#) [\[PubMed\]](#)
- Rayachoti, E.; Tirumalasetty, S.; Prathipati, S.C. SLT based watermarking system for secure telemedicine. *Clust. Comput.* **2020**, *23*, 1223–1246. [\[CrossRef\]](#)
- Araghi, T.K.; Manaf, A.A. An enhanced hybrid image watermarking scheme for security of medical and non-medical images based on DWT and 2-D SVD. *Future Gener. Comput. Syst.* **2019**, *101*, 1223–1246. [\[CrossRef\]](#)
- Al-Haj, A.; Amer, A. Secured telemedicine using region-based watermarking with tamper localization. *J. Digit. Imaging* **2014**, *27*, 737–750. [\[CrossRef\]](#)
- Gangadhar, Y.; Giridhar Akula, V.; Reddy, P.C. An evolutionary programming approach for securing medical images using watermarking scheme in invariant discrete wavelet transformation. *Biomed. Signal Process. Control* **2018**, *43*, 31–40. [\[CrossRef\]](#)
- Kobayashi, L.O.M.; Furuie, S.S.; Barreto, P.S.L.M. Providing Integrity and Authenticity in DICOM Images: A Novel Approach. *IEEE Trans. Inf. Technol. Biomed.* **2009**, *13*, 582–589. [\[CrossRef\]](#)
- Favorskaya, M.; Savchina, E.; Gusev, K. Feature-based synchronization correction for multilevel watermarking of medical images. *Procedia Comput. Sci.* **2019**, *159*, 1267–1276. [\[CrossRef\]](#)
- Liu, X.; Lou, J.; Fang, H.; Chen, Y.; Ouyang, P.; Wang, Y.; Zou, B.; Wang, L. A Novel Robust Reversible Watermarking Scheme for Protecting Authenticity and Integrity of Medical Images. *IEEE Access* **2019**, *7*, 76580–76598. [\[CrossRef\]](#)
- Mothi, R.; Karthikeyan, M. Protection of bio medical iris image using watermarking and cryptography with WPT. *Measurement* **2019**, *136*, 67–73. [\[CrossRef\]](#)
- Liao, X.; Guo, S.; Yin, J.; Wang, H.; Li, X.; Sangaiah, A.K. New cubic reference table based image steganography. *Multimed. Tools Appl.* **2018**, *77*, 10033–10050. [\[CrossRef\]](#)
- Liao, X.; Yin, J.; Chen, M.; Qin, Z. Adaptive Payload Distribution in Multiple Images Steganography Based on Image Texture Features. *IEEE Trans. Dependable Secur. Comput.* **2022**, *19*, 897–911. [\[CrossRef\]](#)
- Gong, L.H.; Tian, C.; Zou, W.P.; Zhou, N.R. Robust and imperceptible watermarking scheme based on Canny edge detection and SVD in the contourlet domain. *Multimed. Tools Appl.* **2021**, *80*, 439–461. [\[CrossRef\]](#)
- Singh, K.U.; Kumar, A.; Singh, T.; Ram, M. Image-based decision making for reliable and proper diagnosing in NIFTI format using watermarking. *Multimed. Tools Appl.* **2022**, *81*, 39577–39603. [\[CrossRef\]](#)
- Singh, K.U.; Abu-Hamatta, H.S.; Kumar, A.; Singhal, A.; Rashid, M.; Bashir, A. Secure watermarking scheme for color DICOM images in telemedicine applications. *Comput. Mater. Contin.* **2022**, *70*, 2525–2542.
- Ali, Z.; Imran, M.; McClean, S.; Khan, N.; Shoaib, M. Protection of records and data authentication based on secret shares and watermarking. *Future Gener. Comput. Syst.* **2019**, *98*, 331–341. [\[CrossRef\]](#)
- Singh, L.; Singh, A.K.; Singh, P.K. Secure data hiding techniques: A survey. *Multimed. Tools Appl.* **2020**, *79*, 15901–15921. [\[CrossRef\]](#)
- Qasim, A.F.; Meziane, F.; Aspin, R. Digital watermarking: Applicability for developing trust in medical imaging workflows state of the art review. *Comput. Sci. Rev.* **2018**, *27*, 45–60. [\[CrossRef\]](#)
- Hurrah, N.N.; Parah, S.A.; Loan, N.A.; Sheikh, J.A.; Elhoseny, M.; Muhammad, K. Dual watermarking framework for privacy protection and content authentication of multimedia. *Future Gener. Comput. Syst.* **2019**, *94*, 654–673. [\[CrossRef\]](#)
- Saxena, N.; Mishra, K.K. Improved multi-objective particle swarm optimization algorithm for optimizing watermark strength in color image watermarking. *Appl. Intell.* **2017**, *47*, 362–381. [\[CrossRef\]](#)
- Su, Q.; Chen, B. Robust color image watermarking technique in the spatial domain. *Soft Comput.* **2018**, *22*, 91–106. [\[CrossRef\]](#)
- Abdallah, E.E.; Ben Hamza, A.; Bhattacharya, P. Watermarking 3D models using spectral mesh compression. *Signal Image Video Process.* **2009**, *3*, 375–389. [\[CrossRef\]](#)
- Selesnick, I. The slantlet transform. *IEEE Trans. Signal Process.* **1999**, *47*, 1304–1313. [\[CrossRef\]](#)
- Liu, D.; Yuan, Z.; Su, Q. A blind color image watermarking scheme with variable steps based on Schur decomposition. *Multimed. Tools Appl.* **2020**, *79*, 7491–7513. [\[CrossRef\]](#)

26. Hsu, L.Y.; Hu, H.T. Robust blind image watermarking using crisscross inter-block prediction in the DCT domain. *J. Vis. Commun. Image Represent.* **2017**, *46*, 33–47. [[CrossRef](#)]
27. Balasamy, K.; Ramakrishnan, S. An intelligent reversible watermarking system for authenticating medical images using Wavelet and PSO. *Clust. Comput.* **2019**, *22*, 4431–4442. [[CrossRef](#)]
28. Sisaudia, V.; Vishwakarma, V.P. Copyright protection using KELM-PSO based multi-spectral image watermarking in DCT domain with local texture information based selection. *Multimed. Tools Appl.* **2021**, *80*, 8667–8688. [[CrossRef](#)]
29. Zhang, Y.; Wang, S.; Ji, G. A Comprehensive Survey on Particle Swarm Optimization Algorithm and Its Applications. *Math. Probl. Eng.* **2015**, *2015*, 931256. [[CrossRef](#)]
30. Singh, K.U.; Kumar, L.; Bhatia, S.; Kumar, A.; Almutairi, A.K.; Shah, M.A. ROI-Fuzzy Based Medical Data Authentication Scheme for Smart Healthcare System. *IEEE Access* **2022**, *10*, 132121–132131. [[CrossRef](#)]
31. Pallaw, V.K.; Singh, K.U.; Kumar, A.; Singh, T.; Swarup, C.; Goswami, A. A Robust Medical Image Watermarking Scheme Based on Nature-Inspired Optimization for Telemedicine Applications. *Electronics* **2023**, *12*, 334. [[CrossRef](#)]
32. Kang, X.; Chen, Y.; Zhao, F.; Lin, G. Multi-dimensional particle swarm optimization for robust blind image watermarking using intertwining logistic map and hybrid domain. *Soft Comput.* **2020**, *24*, 10561–10584. [[CrossRef](#)]
33. Wang, D.; Yang, F.; Zhang, H. Blind color image watermarking based on DWT and LU decomposition. *J. Inf. Process. Syst.* **2016**, *12*, 765–778.
34. Yaqub, M.; Jinchao, F.; Ahmed, S.; Arshid, K.; Bilal, M.A.; Akhter, M.P.; Zia, M.S. GAN-TL: Generative Adversarial Networks with Transfer Learning for MRI Reconstruction. *Appl. Sci.* **2022**, *12*, 8841. [[CrossRef](#)]
35. Dharejo, F.A.; Zawish, M.; Deebea, F.; Zhou, Y.; Dev, K.; Khowaja, S.A.; Qureshi, N.M.F. Multimodal-Boost: Multimodal Medical Image Super-Resolution Using Multi-Attention Network With Wavelet Transform. *IEEE/ACM Trans. Comput. Biol. Bioinform.* **2022**, 1–14. [[CrossRef](#)]
36. Calisto, F.M.; Nunes, N.; Nascimento, J.C. BreastScreening: On the Use of Multi-Modality in Medical Imaging Diagnosis. In Proceedings of the AVI '20: International Conference on Advanced Visual Interfaces, Salerno, Italy, 28 September–2 October 2020; Association for Computing Machinery: New York, NY, USA, 2020. [[CrossRef](#)]
37. Kalra, G.S.; Talwar, R.; Sadawarti, H. Adaptive digital image watermarking for color images in frequency domain. *Multimed. Tools Appl.* **2015**, *74*, 6849–6869. [[CrossRef](#)]
38. Ali, M.; Ahn, C.W. An optimized watermarking technique based on self-adaptive DE in DWT-SVD transform domain. *Signal Process.* **2014**, *94*, 545–556. [[CrossRef](#)]
39. Kazemivash, B.; Moghaddam, M.E. A predictive model-based image watermarking scheme using Regression Tree and Firefly algorithm. *Soft Comput.* **2018**, *22*, 4083–4098. [[CrossRef](#)]
40. Moeinaddini, E. Selecting optimal blocks for image watermarking using entropy and distinct discrete firefly algorithm. *Soft Comput.* **2019**, *23*, 9685–9699. [[CrossRef](#)]
41. Pourhadi, A.; Mahdavi-Nasab, H. A robust digital image watermarking scheme based on bat algorithm optimization and SURF detector in SWT domain. *Multimed. Tools Appl.* **2020**, *79*, 21653–21677. [[CrossRef](#)]
42. Rajpal, A.; Mishra, A.; Bala, R. Multiple scaling factors based Semi-Blind watermarking of grayscale images using OS-ELM neural network. In Proceedings of the 2016 IEEE International Conference on Signal Processing, Communications and Computing (ICSPCC), Hong Kong, China, 5–8 August 2016; pp. 1–6. [[CrossRef](#)]
43. Sharma, V.; Mir, R.N. An enhanced time efficient technique for image watermarking using ant colony optimization and light gradient boosting algorithm. *J. King Saud Univ.-Comput. Inf. Sci.* **2022**, *34*, 615–626. [[CrossRef](#)]
44. Okuwobi, I.P.; Ding, Z.; Wan, J.; Jiang, J. SWM-DE: Statistical wavelet model for joint denoising and enhancement for multimodal medical images. *Med. Nov. Technol. Devices* **2023**, *18*, 100234. [[CrossRef](#)]
45. Eberhart, R.; Kennedy, J. A new optimizer using particle swarm theory. In Proceedings of the MHS'95: Sixth International Symposium on Micro Machine and Human Science, Nagoya, Japan, 4–6 October 1995; pp. 39–43.
46. Daubechies, I.; Sweldens, W. Factoring wavelet transforms into lifting steps. *J. Fourier Anal. Appl.* **1998**, *4*, 247–269. [[CrossRef](#)]
47. Verma, V.S.; Kumar Jha, R. Improved watermarking technique based on significant difference of lifting wavelet coefficients. *Signal Image Video Process.* **2015**, *9*, 1443–1450. [[CrossRef](#)]
48. Chen, D.Y.; Ouhyoung, M.; Wu, J.L. A shift-resisting public watermark system for protecting image processing software. *IEEE Trans. Consum. Electron.* **2000**, *46*, 404–414. [[CrossRef](#)]
49. Golub, G.; Nash, S.; Van Loan, C. A Hessenberg-Schur method for the problem $AX + XB = C$. *IEEE Trans. Autom. Control.* **1979**, *24*, 909–913. [[CrossRef](#)]
50. Sui, L.; Gao, B. Color image encryption based on gyator transform and Arnold transform. *Opt. Laser Technol.* **2013**, *48*, 530–538. [[CrossRef](#)]
51. Kutter, M.; Petitcolas, F.A.P. Fair benchmark for image watermarking systems. *Proc. SPIE* **1999**, *3657*, 226–239. [[CrossRef](#)]
52. Wang, Z.; Bovik, A.C.; Sheikh, H.R. Structural similarity based image quality assessment. In *Digital Video Image Quality and Perceptual Coding*; CRC Press: Boca Raton, FL, USA, 2017; pp. 225–242.
53. Padhye, N.; Branke, J.; Mostaghim, S. Empirical comparison of MOPSO methods—Guide selection and diversity preservation. In Proceedings of the 2009 IEEE Congress on Evolutionary Computation, Trondheim, Norway, 18–21 May 2009; pp. 2516–2523. [[CrossRef](#)]

54. Padhye, N. Comparison of Archiving Methods in Multi-Objectiveparticle Swarm Optimization (MOPSO): Empirical Study. In Proceedings of the GECCO '09: 11th Annual Conference on Genetic and Evolutionary Computation, Montreal, QC, Canada, 8–12 July 2009; Association for Computing Machinery: New York, NY, USA, 2009; pp. 1755–1756. [[CrossRef](#)]
55. Alvarez-Benitez, J.E.; Everson, R.M.; Fieldsend, J.E. A MOPSO Algorithm Based Exclusively on Pareto Dominance Concepts. In Proceedings of the Evolutionary Multi-Criterion Optimization, Guanajuato, Mexico, 9–11 March 2005; Coello Coello, C.A., Hernández Aguirre, A., Zitzler, E., Eds.; Springer: Berlin/Heidelberg, Germany, 2005; pp. 459–473.
56. Hu, W.; Yen, G.G. Density estimation for selecting leaders and mantaining archive in MOPSO. In Proceedings of the 2013 IEEE Congress on Evolutionary Computation, Cancun, Mexico, 20–23 June 2013; pp. 181–188.

Disclaimer/Publisher’s Note: The statements, opinions and data contained in all publications are solely those of the individual author(s) and contributor(s) and not of MDPI and/or the editor(s). MDPI and/or the editor(s) disclaim responsibility for any injury to people or property resulting from any ideas, methods, instructions or products referred to in the content.